Directional crack propagation of granular water systems

Tsuyoshi Mizuguchi*
Department of Mathematical Sciences, Osaka Prefecture University, Sakai 599-8531, Japan

Akihiro Nishimoto
Department of Physics, Kyoto University, Kyoto 606-8502, Japan

So Kitsunezaki
Graduate School of Human Culture, Nara Women's University, Nara 630-8506, Japan

Yoshihiro Yamazaki
Department of Physics, Waseda University, Tokyo 169-8555, Japan

Ichio Aoki
Department of Medical Informatics, Meiji University of Oriental Medicine, Kyoto 629-0392, Japan
(Received 29 December 2004; published 27 May 2005)

Pattern dynamics of directional crack propagation phenomena observed in drying process of starch-water mixture is investigated. To visualize the three-dimensional structure of the drying-fracture process two kinds of experiments are performed, i.e., resin solidification planing method and real-time measurement of water content distribution with MR instruments. A cross section with polygonal structure is visualized in both experiments. The depth dependency of cell size is measured. The phenomenological model for water transportation is also discussed.

DOI: 10.1103/PhysRevE.71.056122 PACS number(s): 62.20.Mk, 46.50.+a, 81.40.Np

I. INTRODUCTION

Pattern formations of cracks are common phenomena in daily life and are well studied in various fields [1]. The elementary process is, however, fracture, which has high nonlinearity and irreversibility and is not well understood. Among these fracture phenomena, gradients of external field, such as temperature or water content, cause directional propagation of cracks along the gradient with low tip velocity compared to the sound velocity of the material. Cracks made by such a fracture process often show regular structure. Dynamics and morphology of directional crack propagation in a pseudo-two-dimensional system are well studied for cooled glass plates [2–4] or the drying process of colloidal suspension [5]. For the three-dimensional case, on the other hand, besides cooling glass experiments [6] or mathematical models [7], the most intriguing example is *columnar joints*, a spectacle polygonal columnar structure found in cooled basaltic lava. Most of them, however, are reports based on the observations and theoretical modelings [8–11]. Difficulties in realization of physical condition and visualization prevents us from experimental study.

Recently a prismal structure similar to that of the columnar joint is demonstrated in the drying process of a starch-water mixture [12–16]. Analyses, however, such as morphology of cross section, time development of crack pattern, and relation between them, are not performed in detail. In this paper, we report visualization methods of pattern-formation phenomena of shrinkage crack during the drying process of a starch-water mixture system. First, we study the static pattern of a crack after the drying process by the resin solidification planing (RSP) method. Second, real-time measurement of water content distribution is reported. Finally, we present a model of water transportation considering a bulk diffusion in porous media and a drainage effect of cracks.

II. STATIC PATTERNS

The experimental procedure is typically as follows: As a sample, starch (corn) and water of the same mass are mixed and poured into a glass or acrylic container of which the upper side remains open. The sample is dried in an electric furnace or air-conditioned room in which the temperature is controlled by a feedback circuit. Drying causes local volume contraction in the sample and stress concentration accompanied with the shrinkage process is released by crack formation. About the starch-water system, the following results are observed typically [1,12–15]. If the sample is thin, e.g., the aspect ratio is larger than 10, two types of cracks are observed as shown in Fig. 1. The smooth cracks are called type I and sinuous ones are called type II, which have the following differences in morphological and dynamical properties: (i) Type I is formed before type II emerges. (ii) Type I shows uniform structure along vertical direction except a microscopic plumose pattern on the surface. Type II, on the contrary, shows obvious three dimensionality and prismal structure with polygonal cross sections are observed, as will be described later. (iii) The dynamical process of each type is different; each type I crack is formed sequentially, i.e.,

*Electronic address: gutchi@ms.osakafu-u.ac.jp

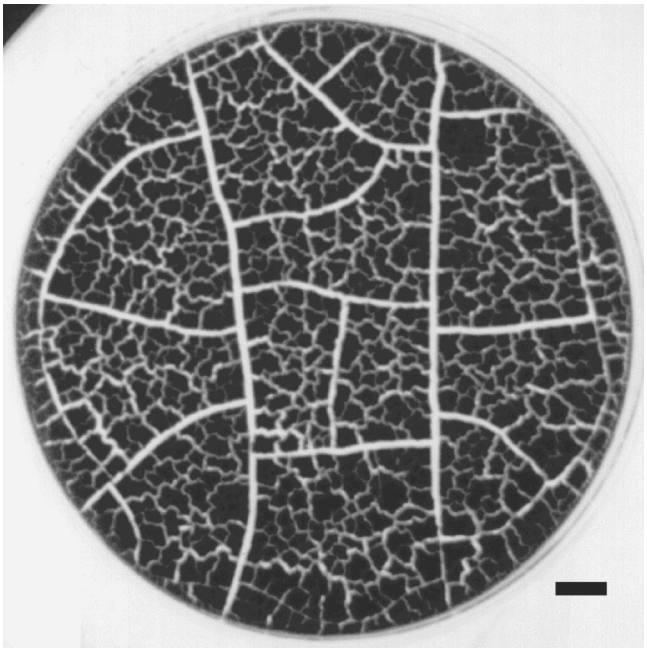

FIG. 1. Visualization from the top with transparent light. Bar denotes 10 mm. The depth of sample is 5 mm.

"branch" ran after "trunk" [17]. On the other hand, the formation process of type II is considered that the pattern emerges at the surface simultaneously and it propagates inwardly. (iv) About the origin of the stress concentration, type I is made by the difference of contraction ratio between the mixture and the container and frictional force between them [18–21]. Type II is considered to be made by the nonuniformity of the local shrinkage in the mixture.

We now focus on the visualization of type II cracks. Besides breaking the sample manually or by x-ray computer tomography, the three-dimensional structure of type II cracks is visualized by the resin solidification planing (RSP) method. RSP method is as follows: after the drying process the sample is solidified with an epoxy resin (STYCAST 1266) with a few drops of ink for visualization, and the cross section is observed by planing away by a lathe. Each cross section is recorded by a scanner with 600 dpi and 256 gray scale. Corn starch (Nacalai Tesque) is used and the aspect ratio of the sample is taken to be ~ 1 in order to decrease the number of type I cracks by considering that typical spacing of type I is proportional to the sample thickness [18,19]. Figure 2 shows typical cross sections. The vertical section shows that several cracks stop to propagate at some depth, and spacing between cracks widens as it deepens [Fig. 2(a)]. The horizontal sections visualize the clear polygonal structure. The deeper section shows a similar pattern with increasing characteristic size compared to the shallower one, as shown in Figs. 2(b) and 2(c). Rearrangement of crack networks is observed in the form of cell fusion or an edge-shortening process. Both sections show that the characteristic size of polygons is the increasing function of depth z from the surface. This tendency is quantified by measuring the total crack length at each depth. The crack length $L(z)$ is determined by the total area of the image after thresholding and skeletonizing raw data of that depth z. $L(z)$ is a decreasing function, and it has a form $\propto z^{-0.79\pm0.4}$ if we try to fit for the deep region [Fig. 2(d)]. Assuming the geometric relation that the polygonal cell has the same shape and same size in the horizontal section, the size of cell b is related to L in the form $b \sim L^{-1}$. Therefore b increases with the depth. The distribution function of the angle between cracks has a single peak near 120° as in Fig. 2(e) [22,23].

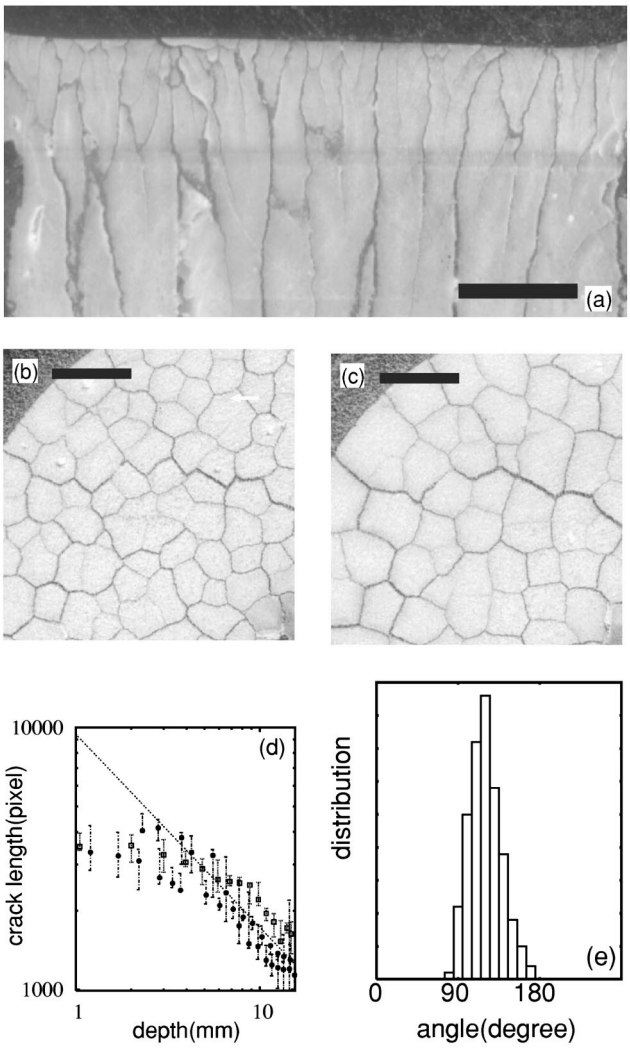

FIG. 2. (a) Vertical section parallel to the z axis. Horizontal sections at 6.25 mm (b) and 11.60 mm (c) depth from the surface. Each bar denotes 5 mm. (d) Depth vs total crack length. The line shows the result of fitting for the deep region. (e) Distribution of angle between cracks in horizontal slices.

III. DYNAMICAL BEHAVIOR

To clarify the mechanism of crack formation we perform direct measurement of water content distribution, which is considered to cause the stress concentration. From the results of preliminary experiments, the following three stages are observed during the drying process. *Stage 1*: Water content decreases uniformly. *Stage 2*: A sudden change of water content occurs and type I cracks are formed mainly between the

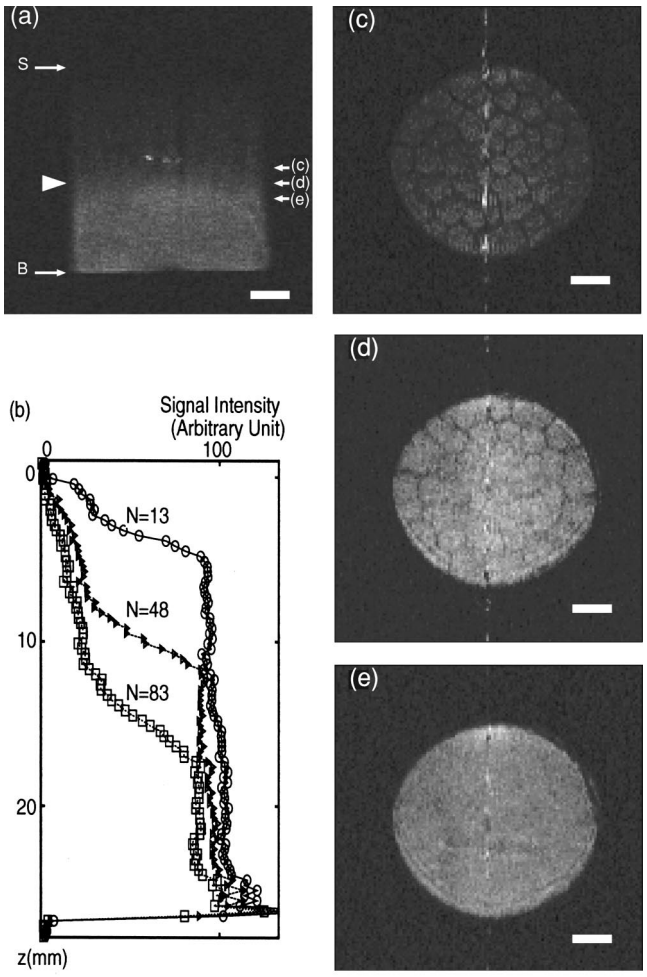

FIG. 3. (a) MR image of vertical section of the sample at $N=83$. White bar represents 5 mm length. Arrows with S and B denote the position of the surface and the bottom, respectively. Water content shock locates near the white triangle. The symbols (c), (d), and (e) represent the position of horizontal slices, which is indicated by the same symbol. (b) Snapshots of signal intensity along vertical direction. The vertical axis corresponds to the depth from the surface and horizontal axis represents the intensity. Horizontal images (c), (d), and (e) are averaged snapshots around $N=83$ at the position indicated by the symbol in (a).

mixture and the side wall of the container. An influence on the side wall of the container, such as friction, can be negligible for the later process because they detach from each other at this time. The distribution remains approximately uniform. *Stage 3*: The water content decreases slowly. The distribution is *not* uniform but it exhibits "front," which sweeps the sample from the surface to inside as shown later. We focus on the stage 3, which is considered to be the formation process of type II cracks.

MR experiments were performed on a 4.7 T horizontal spectrometer (CSI-II-Omega, Bruker, Germany) equipped with a shielded gradient coil of 65 mm in diameter (ID = 65 mm, SR-65, Bruker). Three sets of multislice Gradient-echo (GE) images, vertical plane, horizontal plane without slice offset, and horizontal plane with slice offset, were sequentially obtained during the drying process. The image of vertical plane was measured using the following parameters: pulse repetition time (TR) = 100 ms, echo time (TE) = 2.9 ms, matrix size = 128×128, flip angle = 90°, field of view (FOV) = 40 mm, slice thickness (ST) = 6 mm, number of slices = 1, number of averages (NA) = 32, and acquisition time of vertical plane was ~7 min. The images of horizontal plane with and without slice offset were detected using the following parameters: TR = 320 ms, TE = 2.9 ms, matrix size = 128×128, flip angle = 90°, FOV = 40 mm, ST = 2 mm, slice gap = 2 mm, number of slices = 8, slice offset = 0 or 2 mm, NA = 46, and acquisition time of horizontal plane was ~31 min for each. Therefore, the total acquisition time of T_1-weighted image was 69 min. The acquisition were repeated 87 times for ~100 h continuously during the drying process. Finally, 87 sets of T_1-weighted images were acquired in all. The signal detected by GE sequence with short-TE and short-TR mostly reflects proton distribution of water in the sample. However, the contribution of proton that has a long T_1 relaxation time, such as free water, is estimated low using this sequence; it has a small contribution at the sample after predrying (data not shown). Therefore, one can say that the signal intensity of the MR images depends on the proton distribution of water at this imaging parameter and sample condition. The temperature of the sample are regulated to 25 °C by an electric dryer with feedback from the thermometer near the sample. Image analysis was performed using MRVision (MRVision Co., MA), NIH Image (NIH, MD), and ImageJ (NIH). Data are presented as mean plus or minus standard deviation (SD).

Figure 3 shows typical snapshots in stage 3. The Nth acquisition, i.e., $N \times 69$ min later from the beginning of stage 3 is numbered as N. Vertical slice at $N=83$ shows the water content distribution, which has a front [Fig. 3(a)]. Several snapshots of vertical distribution of water content by averaging the gray scale over horizontal direction are plotted for $N=13$, 48, and 83 as shown in Fig. 3(b). Following properties are worth noting: (i) The front of water content propagates inwardly with decreasing its velocity. (ii) The distribution function $C(z,t)$ has a concave regime, i.e., $d^2C/dz^2>0$ above the front. (iii) The gradient of water content at the front decreases with depth and time. Horizontal slices, Figs. 3(c)–3(e), are snapshots of the same time as 3(a). To improve the signal-to-noise ratio, seven sets of horizontal images were averaged, retrospectively. Therefore, temporal resolution of horizontal images was 3.5 h. This averaging was not applied for the vertical images. Polygonal structures, which well coincide with those of cracks observed by the RSP method, are observed at and above the front, as shown in Figs. 3(c) and 3(d). Below the front, on the contrary, the distribution is uniform [Fig. 3(e)]. At the different time, the same structures are observed, except for the position of the front and the characteristic size of polygons. From these observations it is suggested that (S1) cracks are formed at the front and (S2) cracks play role as drainage for water transportation. It should be noted that the images do not visualize the crack itself because the signal reflects the water content and it expresses neither stress nor strain.

IV. MODEL OF WATER TRANSPORTATION

We now give an interpretation about the data taken from the experiments and consideration on the crack-forming

mechanism. First, we refer to dependence among crack, stress, and water content, which is the main driving factor. As the same in the general fracture phenomena, crack and stress have mutual influence and must be solved as order parameters or boundary conditions depending on space and time. As for the three-dimensional case as in this experiment (and the columnar joint), the external field should be solved as another order parameter. Especially, if the cracks play role of drainage as suggested by Figs. 2 and 3, water content distribution is affected by the cracks made up to that time and is not solved independently.

So we discuss the evolution of water content distribution. The change of water content distribution consist of various elementary processes, such as transportation of liquid water; vapor and heat, and evaporation in porous media. Standard theory contains a lot of coefficients, depending on the materials [24]. Here, we focus on two effects, i.e., transportation in bulk porous media and drainage effect through the cracks. The former is a water transportation process in nonuniform unsaturated porous medium and generally depends on the temperature gradient and gradient of water volume fraction C. Assuming that the temperature is almost constant, C obeys Richardson's diffusion equation by applying extended Darcy's law, the latter depends on the configuration of crack networks at that time and the difference $C_o - C$, where C_o is a saturated water volume fraction at which a net evaporation flow disappear [25]. Therefore, an evaporation speed per unit area through the crack is considered to be $\lambda(C_o - C)$, where λ is the coefficient of mass transfer. Note that C_o is a function of z because it depends on the water vapor pressure in the crack.

Now, we consider the one-dimensional problem. Let the vertical distribution function of water volume fraction averaged in the horizontal direction be $\overline{C}(z,t)$, i.e., $\overline{C}(z,t) \equiv \int\int C(x,y,z,t)dx\,dy/A$, where $C(x,y,z,t)$ is a three-dimensional distribution function of water volume fraction and A is an area of base of the sample. Next, let the length of type II crack per unit area at depth z and time t be $\tilde{L}(z,t) \equiv L(z,t)/A$, where $L(z,t)$ is a total length of type II crack. Then the evaporation through the crack is represented as $\lambda(C_o - \overline{C})\tilde{L}$. We obtain the evolution equation for $\overline{C}(z,t)$

$$\frac{\partial \overline{C}}{\partial t} = \frac{\partial}{\partial z}\left(D\frac{\partial \overline{C}}{\partial z}\right) + \lambda(C_o - \overline{C})\tilde{L}. \tag{1}$$

In general, the diffusion coefficient D and saturated volume fraction C_o are not constant, i.e., D is a function of C while C_o depends on z. Unless the spatiotemporal pattern of crack $\tilde{L}(z,t)$ is given, the evolution equation cannot be solved. Here, we consider two extreme cases. If the second term of Eq. (1) is negligible, then the water transportation is mainly carried by the diffusion in the bulk porous media. In this case the concaveness of $\overline{C}$ shown in Fig. 3(b) is considered to originate from the C dependency of the diffusion coefficient $D(C)$, i.e., nonlinear diffusion. On the contrary, if the first term is negligible, then the evaporation through the cracks governs the evolution. Especially, if C_o is constant, then the outside of the crack is as dry as it is above the surface. In this case, there is a steady propagating solution in which the stress distribution by the local shrinkage holds a definite shape relative to the crack tip. This is a kind of "self-driven crack" [26,27] and it is expected that $\tilde{L}$ does not depend on z. From the experimental results that the cellular structure is observed in the water content distribution [Figs. 3(c) and 3(d)] and $\tilde{L}$ is decreasing function of z as shown in Fig. 2(d), the actual water content distribution is considered to evolve with C dependency of diffusion coefficient $D(C)$ or z dependency of water vapor pressure $C_o(z)$ or a composition of both effects.

V. CONCLUSION

We study the formation process of columnar structures by the directional crack propagation phenomena observed in the drying process of a starch-water mixture. The three-dimensional structures are visualized by two different methods. The RSP method clarifies the static pattern of the crack network with polygonal cross section after the drying process. The MR experiments exhibit the dynamical behavior of the sweeping front of the water content at which the polygonal structures are formed during drying by real-time measurement. Finally, we suggest a model for the water transportation in the sample that consists of two effects, (nonlinear) diffusion in the bulk porous media and the drainage through the crack networks.

To obtain a closed form of the averaged water content $\overline{C}$ and the crack density $\tilde{L}$, we need an evolution rule for $\tilde{L}$. In the stage 3, the water content of the sample is small and the sample is supposed to be elastic for stress with the time scale of crack forming (at most 10^2 h) [28]. If the fracture process is quasistatic, Griffith criterion can be adopted. Numerical computations will be useful to estimate the elastic energy because it depends on both the geometry of crack networks and the stress distribution. It will be also useful to handle a full three-dimensional model using $C(x,y,z,t)$.

ACKNOWLEDGMENTS

We acknowledge Y. Sasaki for advising about the experimental method. We also thank to Professor M. Sano, Professor Y. Kuramoto, Professor C. Tanaka, Professor K. Fukuda, A. Yuse, T. Segawa, M. Abe, Y. Tanaka, and H. Tanaka for valuable discussions. T.M. thanks Professor A.-H. Bahr and H. Funahashi for fruitful discussions. This work was partially supported by a Grant-in-Aid for Scientific Research (C) No. 16605008 of the Ministry of Education, Culture, Sports, Science and Technology.

[1] J. Walker, Sci. Am. **255**, 178 (1986).
[2] A. Yuse and M. Sano, Nature (London) **362**, 329 (1993).
[3] S. Nemat-Nasser, L. M. Keer, and K. S. Parihar, Int. J. Solids Struct. **14**, 409 (1978).
[4] O. Ronsin and B. Perrin, Phys. Rev. E **58**, 7878 (1998).
[5] C. Allain and L. Limat, Phys. Rev. Lett. **74**, 2981 (1995).
[6] H.-A. Bahr, U. Bahr, A. Gerbatsch, I. Pflugbeil, A. Vojta, and H.-J. Weiss, in *Fracture Mechanics of Ceramics*, edited by R. C. Bradt *et al.* (Plenum Press, New York, 1996), Vol. 11, p. 507.
[7] Y. Hayakawa, Phys. Rev. E **50**, R1748 (1994).
[8] S. Folley, Philos. Trans. R. Soc. London, Ser. A **212**, 170 (1694).
[9] A. Aydin and J. M. DeGraff, Science **239**, 471 (1988).
[10] A. H. Lachenbruch, Spec. Pap. Geol. Soc. Am. **70**, 69 (1962).
[11] E. A. Jagla and A. G. Rojo, Phys. Rev. E **65**, 026203 (2002).
[12] G. Müller, J. Volcanol. Geotherm. Res. **86**, 93 (1998).
[13] G. Müller, J. Geophys. Res. **103**, 15239 (1998).
[14] T. Mizuguchi, A. Nishimoto, S. Kitsunezaki, Y. Yamazaki, and I. Aioki, in *Powders and Grains 2001*, edited by Y. Kishino (Balkema, Lisse, 2001), p. 55.
[15] A. Toramaru and T. Matsumoto, J. Geophys. Res. **109**, B02205 (2004).
[16] L. Goehring and S. W. Morris, Europhys. Lett. **69**, 739 (2005).
[17] Because the crack tip has a finite propagation velocity, the order of emergence of type I cracks is defined locally. The crack tip may collide its own tail.
[18] A. Groisman and E. Kaplan, Europhys. Lett. **25**, 415 (1994).
[19] S. Kitsunezaki, Phys. Rev. E **60**, 6449 (1999).
[20] K. T. Leung and Z. Neda, Phys. Rev. Lett. **85**, 662 (2000).
[21] K. A. Shorlin, J. R. de Bruyn, M. Graham, and S. W. Morris, Phys. Rev. E **61**, 6950 (2000).
[22] The "angle" between cracks must be defined carefully. In this letter, thresholding and skeletonization procedure makes raw data into a set of curves, which is regarded as the trace of crack tip. A circle with radius r_0 is drawn at the three-handed vertex, and the ratio of the angles around that vertex are defined by the ratio of area of circular arc devided by the curves. The singleness and the position of the peak is robust against r_0 in appropriate range.
[23] The estimation of the number of polygone sides also requires circumspection because there are many cracks which end does not connect to other.
[24] F. A. L. Dullien, *Porous Media* (Academic Press, New York, 1979).
[25] T. S. Komatsu, J. Phys. Soc. Jpn. **70**, 3755 (2001).
[26] B. I. Yakobson, Phys. Rev. Lett. **67**, 1590 (1991).
[27] T. Boeck, H.-A. Bahr, S. Lampensherf, and U. Bahr, Phys. Rev. E **59**, 1408 (1999).
[28] There remains a possibility that a memory effect due to viscoelasticity makes influence to the crack pattern formation process, e.g., A. Nakahara and Y. Matsuo J. Phys. Soc. Jpn. **74**, 1362 (2005).